Supplementary Material

Shifts in water supply and demand drive land cover change across Chile

Francisco Zambrano[a,b,*], Anton Vrieling[c], Francisco Meza[d,e,f], Iongel Duran-Llacer[g], Francisco Fernández[h,i], Alejandro Venegas-González[j], Nicolas Raab[d], Dylan Craven[l,m]

[a]*Hémera Centro de Observación de la Tierra, Facultad de Ciencias, Escuela de Ingeniería en Medio Ambiente y Sustentabilidad, Universidad Mayor, Santiago, 7500994, Chile.,*

[b]*Observatorio de Sequía para la Agricultura y la Biodiversidad de Chile (ODES), Universidad Mayor, Santiago, 7500994, Chile.,*

[c]*Faculty of Geo-Information Science and Earth, University of Twente, Enschede, The Netherlands.,*

[d]*Facultad de Agronomía y Sistemas Naturales, Pontificia Universidad Católica de Chile., Santiago, Chile.,*

[e]*Instituto para el Desarrollo Sustentable. Pontificia Universidad Católica de Chile, Santiago, Chile.,*

[f]*Centro Interdisciplinario de Cambio Global, Pontificia Universidad Católica de Chile, Santiago, Chile.,*

[g]*Hémera Centro de Observación de la Tierra, Facultad de Ciencias, Universidad Mayor„ Santiago, 7500994, Chile.,*

[h]*Center of Economics for Sustainable Development (CEDES), Faculty of Economics and Government, Universidad San Sebastian, Santiago, Chile.,*
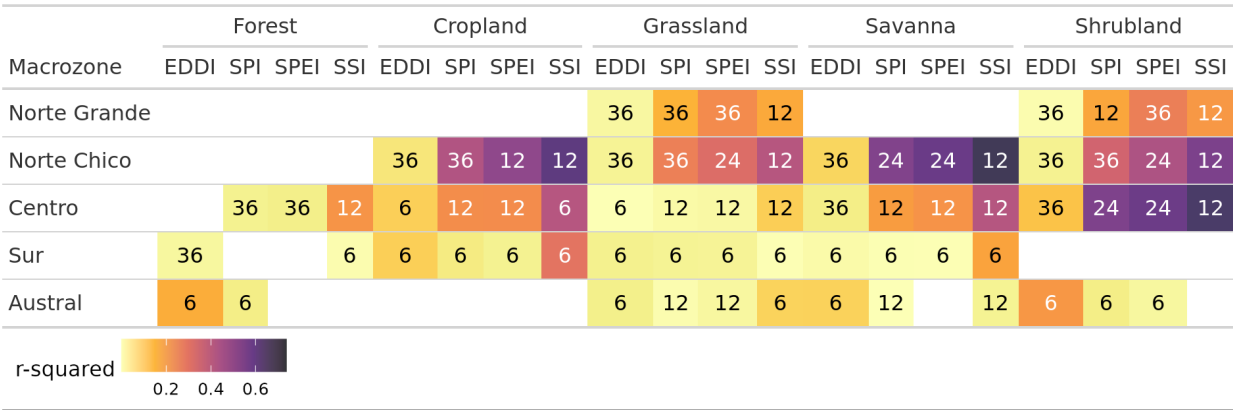
[i]*Center of Applied Ecology and Sustainability (CAPES), Santiago, Chile.,*

[j]*Instituto de Ciencias Agroalimentarias, Animales y Ambientales (ICA3), Universidad de O'Higgins, San Fernando, Chile.,*

[k]*,*

[l]*, GEMA Center for Genomics, Ecology & Environment, Universidad Mayor, Camino La Pirámide Huechuraba 5750, Santiago, Chile.,*

[m]*Data Observatory Foundation, Santiago, Chile.,*

S1. Results

Macrozone	Forest				Cropland				Grassland				Savanna				Shrubland			
	EDDI	SPI	SPEI	SSI	EDDI	SPI	SPEI	SSI	EDDI	SPI	SPEI	SSI	EDDI	SPI	SPEI	SSI	EDDI	SPI	SPEI	SSI
Norte Grande									36	36	36	12					36	12	36	12
Norte Chico					36	36	12	12	36	36	24	12	36	24	24	12	36	36	24	12
Centro		36	36	12	6	12	12	6	6	12	12	12	36	12	12	12	36	24	24	12
Sur	36			6	6	6	6	6	6	6	6	6	6	6	6	6				
Austral	6	6							6	12	12	6	6	12		12	6	6	6	

r-squared 0.2 0.4 0.6

*Corresponding author

Email address: francisco.zambrano@umayor.cl (Francisco Zambrano)

[!ht]

Product	Sub-product	Variable	Spatial Resolution	Period	Units	Short Name
		Precipitation			mm	P
ERA5L		Maximum temperature	0.1°	1981-2023	°C	T_{max}
		Minimum temperature			°C	T_{min}
		Volumetric Soil Water Content at 1m			$m3/m3$	SM
ERA5L*		Atmospheric Evaporative Demand	0.1°	1981-2023	mm	AED
MODIS	MOD13A3.061	Normalized Difference Vegetation Index	1 km	2000-2023		NDVI
	MCD12Q1.061	land cover IGBP scheme		2001-2022		land cover

*Calculated from maximum and minimum temperatures derived from ERA5L with Eq. **??**.

Table S1: Description of the satellite and reanalysis data used

S2. Data

S3. Validation of ERA5L variables

S3.1. Methods

We compared the ERA5L (Muñoz-Sabater et al., 2021) variables for monthly mean temperature, total precipitation, and volumetric soil water content against values retrieved by weather stations. For temperature and precipitation, we used data from the weather network from the Ministry of Agriculture of Chile (www.agromet.com) between 2015 and 2023. We used 277 stations located throughout Chile. For *in-situ* soil moisture, we used a private soil network that is owned by the agricultural enterprise Garces Fruit (https://garcesfruit.com/), which has 99 stations in Central Chile, located in fields with cherry fruit crops. The sensors are installed at 30, 60, and 90cm and are a Advanced Soil Moisture Sensor model Teros 12 from the METER Group (https://metergroup.com/products/teros-12/). To avoid comparing ERA5L with *in-situ* soil moisture levels caused by irrigation, which are not captured by ERA5L, we used daily data for the year 2022 and the months outside the growing season, May to September.

We selected the following metrics:

$$MAE = \frac{1}{n} \sum |E - S|$$

$$Bias = \frac{\sum E}{\sum S}$$

$$ubRMSE = \sqrt{\frac{\sum \left[(E_i - \overline{E}) - (S_i - \overline{S}) \right]^2}{n}}$$

$$CC = \frac{\sum (S_i - \bar{S})(E_i - \bar{E})}{\sqrt{(Si - \bar{S})^2 (E_i - \bar{E})^2}}$$

MAE: mean absolute error

$bias$: bias

$ubRMSE$: unbiassed root mean squared error

CC: coefficient of correlation

S: value of the variable measure by the weather station

E: value of the variable measure by ERA5L

2

S3.2. Results

30 The average performance metrics of ERA5L over the weather and soil moisture stations are shown in
31 Table S2. In the case of the 97 soil moisture stations, we averaged for the three depths (30, 60, and 90cm)
32 and then compared it with the volumetric water content in the top 100cm of the soil derived from ERA5L.
33 For this case, we made a daily comparison to determine the performance metrics per station, then we
34 averaged the measured soil moisture at the three levels and over all stations.

Table S2: Metrics of performance for the climatic and soil moisture variables from ERA5-Land with data from 277 stations in
Central Chile for temperature and precipitation and 99 stations of soil moisture.

Variable	ubRMSE	MAE	Bias	CC
Temperature	1.06 °C	1.13 °C	1.02	0.96
Precipitation	35.5 mm	28.1 mm	1.93	0.85
Soil Moisture (1m)	0.174 cc/cc	0.167 cc/cc	1.74	0.71

35 **S4. Land cover macroclasses and validation**

36 *S4.1. Methods*

37 To analyze the LULCC, we used the IGBP scheme from the MCD12Q1 Collection 6.1 from MODIS. This
38 product has a yearly frequency from 2001 to 2022. The IGBP defines 17 classes; we regrouped these into
39 ten macroclasses, as follows: classes 1-4 to forest, 5-7 to schrublands, 8-9 to savannas, 10 as grasslands, 11
40 as wetlands, 12 and 14 to croplands, 13 as urban, 15 as snow and ice, 16 as barren, and 17 to water bodies.

41 To assess the accuracy of the regrouped MCD12Q1 land cover maps, we compared the macroclasses with
42 those of a more detailed land cover map made by Zhao et al. (2016) for Chile with samples acquired in the
43 years 2013–2014 (LCChile). The latter has a spatial resolution of 30 m and three hierarchy levels of defined
44 classes; from those, we used level 1, which fits with the macroclass land cover. We chose the years 2013
45 (IGBP2013) and 2014 (IGBP2014) from the land cover macroclasses to compare with LCChile. For this
46 comparison, we used the following procedure:

47 i) we resampled LCChile to the spatial resolution (500m) of the land cover macroclasses using the majority
48 method,
49 ii) we took a random sample of 1000 points within continental Chile and extracted the classes that fell
50 within each point for LCChile, IGBP2013, and IGBP2014; we considered the point extracted from
51 LCChile as the truth and the values from the other two years as predictions.
52 iii) we derived a confusion matrix with the classes extracted from the 1000 points for LCChile, IGBP2013,
53 and IGBP2014; and calculated the performance metrics of accuracy and F1.

$$Accuracy = \frac{TP + TN}{TP + TN + FP + FN} = \frac{correct\ classifications}{all\ classifications}$$

$$F1 = \frac{2 \cdot TP}{2 \cdot TP + FP + FN}$$

55 where TP and FN refer to true positive and false negative, correctly classified classes; TN and FP to
56 true negative and false positive, wrongly classified classes.

57 *S4.2. Results*

58 Our results showed a global accuracy of ~0.82 and a F1 score of ~0.66 between the high resolution landcover
59 (LCChile) and the landcover IGBP from MODIS. Thus, for vegetation, we obtained and use hereafter five
60 macroclasses of land cover from IGBP MODIS: forest, shrubland, savanna, grassland, and croplands (Table
61 S3).

Table S3: Landcover clases from IGBP MODIS and the corresponding macroclasses.

Name	Value	Description	Macroclass
Evergreen Needleleaf Forests	1	Dominated by evergreen conifer trees (canopy >2m). Tree cover >60%.	Forest
Evergreen Broadleaf Forests	2	Dominated by evergreen broadleaf and palmate trees (canopy >2m). Tree cover >60%.	Forest
Deciduous Needleleaf Forests	3	Dominated by deciduous needleleaf (larch) trees (canopy >2m). Tree cover >60%.	Forest
Deciduous Broadleaf Forests	4	Dominated by deciduous broadleaf trees (canopy >2m). Tree cover >60%.	Forest
Mixed Forests	5	Dominated by neither deciduous nor evergreen (40-60% of each) tree type (canopy >2m). Tree cover >60%.	Forest
Closed Shrublands	6	Dominated by woody perennials (1-2m height) >60% cover.	Shrublands
Open Shrublands	7	Dominated by woody perennials (1-2m height) 10-60% cover.	Shrublands
Woody Savannas	8	Tree cover 30-60% (canopy >2m).	Savanna
Savannas	9	Tree cover 10-30% (canopy >2m).	Savanna
Grasslands	10	Dominated by herbaceous annuals (<2m).	Grassland
Permanent Wetlands	11	Permanently inundated lands with 30-60% water cover and >10% vegetated cover.	Wetland
Croplands	12	At least 60% of area is cultivated cropland.	Cropland
Urban and Built-up Lands	13	At least 30% impervious surface area including building materials, asphalt, and vehicles.	Urban
Cropland/Natural Vegetation Mosaics	14	Mosaics of small-scale cultivation 40-60% with natural tree, shrub, or herbaceous vegetation.	Cropland
Permanent Snow and Ice	15	At least 60% of area is covered by snow and ice for at least 10 months of the year.	Snow/Ice
Barren	16	At least 60% of area is non-vegetated barren (sand, rock, soil) areas with less than 10% vegetation)	Barren land
Water Bodies	17	At least 60% of area is covered by permanent water bodies	Water
Unclassified	255	Has not received a map label because of missing inputs	Unclassified

S5. Relationship between drought indices and land cover change

Figure S1 shows the ranking of variable importance obtained with the ten folds used in the resampling of the Random Forest model per land cover type.

S6. Trend of vegetation productivity

Figure S2 shows the average trend for zcNDVI for 2000-2023 per macrozone and landcover macroclass.

S7. Vegetation productivity

We analyzed the correlation of zcNDVI for time scales of 1, 3, 6, and 12 months versus net primary production (NPP). We obtained both the zcNDVI from MOD13A3.061 and the NPP from MOD17A3HGF.061, using MODIS products. We used the zcNDVI in December to correlate with the annual NPP. Figure S3 shows a map of the r-squared correlation between zcNDVI and NPP, and Figure S4 shows the aggregated values per macrozone.
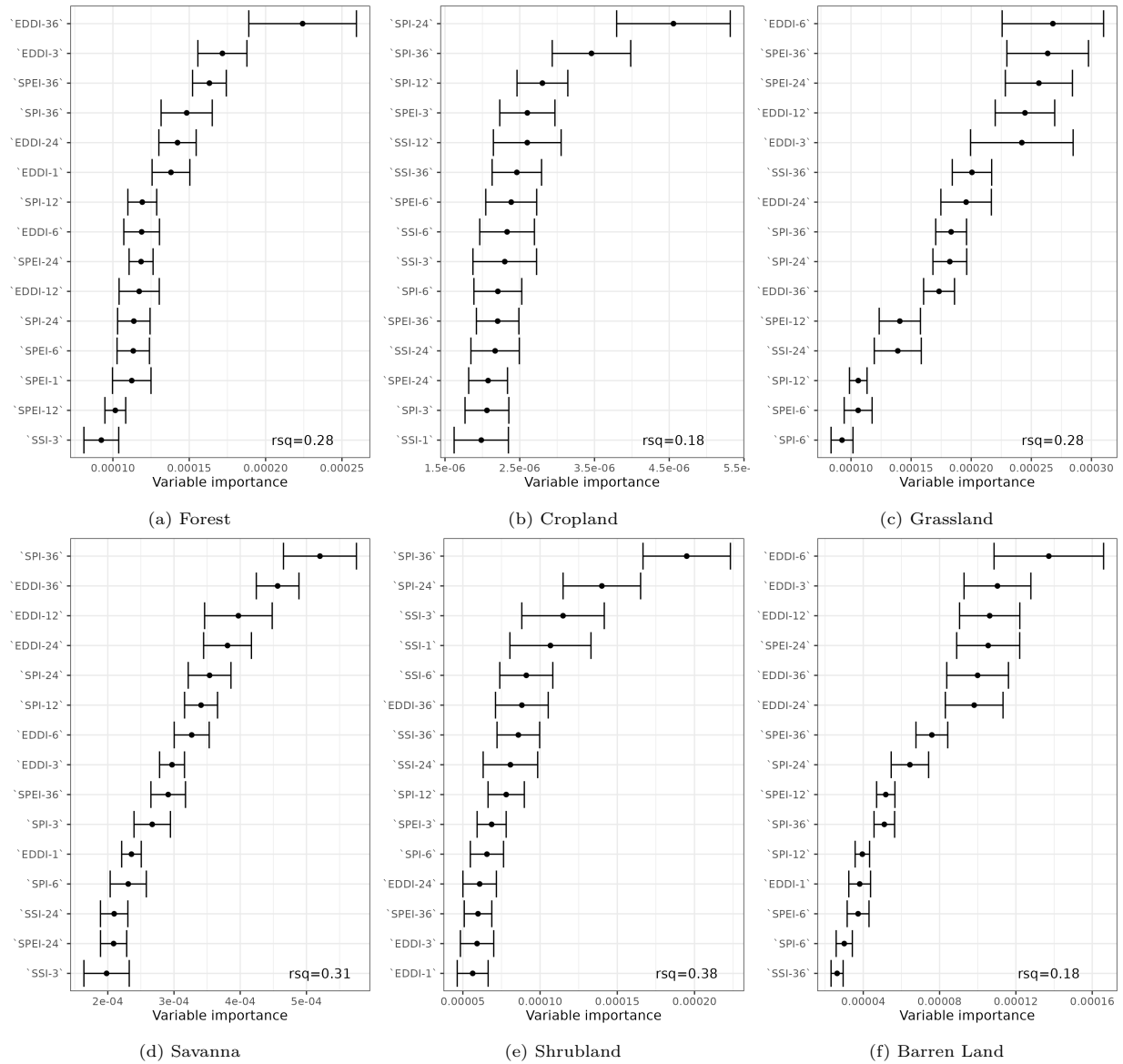
4

Figure S1: Error bar for the variables importance obtained from the 10 resamples folded by the random forest used to model land cover trend using as predictors the trend in drought indices of water supply, water demand, soil moisture, and vegetation productivity.

References

Muñoz-Sabater, J., Dutra, E., Agustí-Panareda, A., Albergel, C., Arduini, G., Balsamo, G., Boussetta, S., Choulga, M., Harrigan, S., Hersbach, H., Martens, B., Miralles, D.G., Piles, M., Rodríguez-Fernández, N.J., Zsoter, E., Buontempo, C., Thépaut, J.N., 2021. ERA5-Land: a state-of-the-art global reanalysis dataset for land applications. Earth System Science Data 13, 4349–4383. URL: https://essd.copernicus.org/articles/13/4349/2021/, doi:10.5194/essd-13-4349-2021.

Zhao, Y., Feng, D., Yu, L., Wang, X., Chen, Y., Bai, Y., Hernández, H.J., Galleguillos, M., Estades, C., Biging, G.S., Radke, J.D., Gong, P., 2016. Detailed dynamic land cover mapping of Chile: Accuracy improvement by integrating multi-temporal data. Remote Sensing of Environment 183, 170–185. URL: https://linkinghub.elsevier.com/retrieve/pii/S0034425716302188, doi:10.1016/j.rse.2016.05.016.
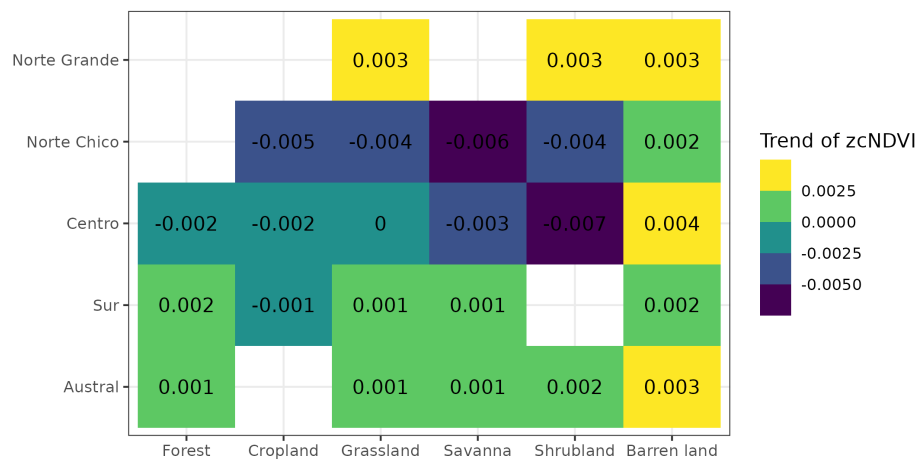
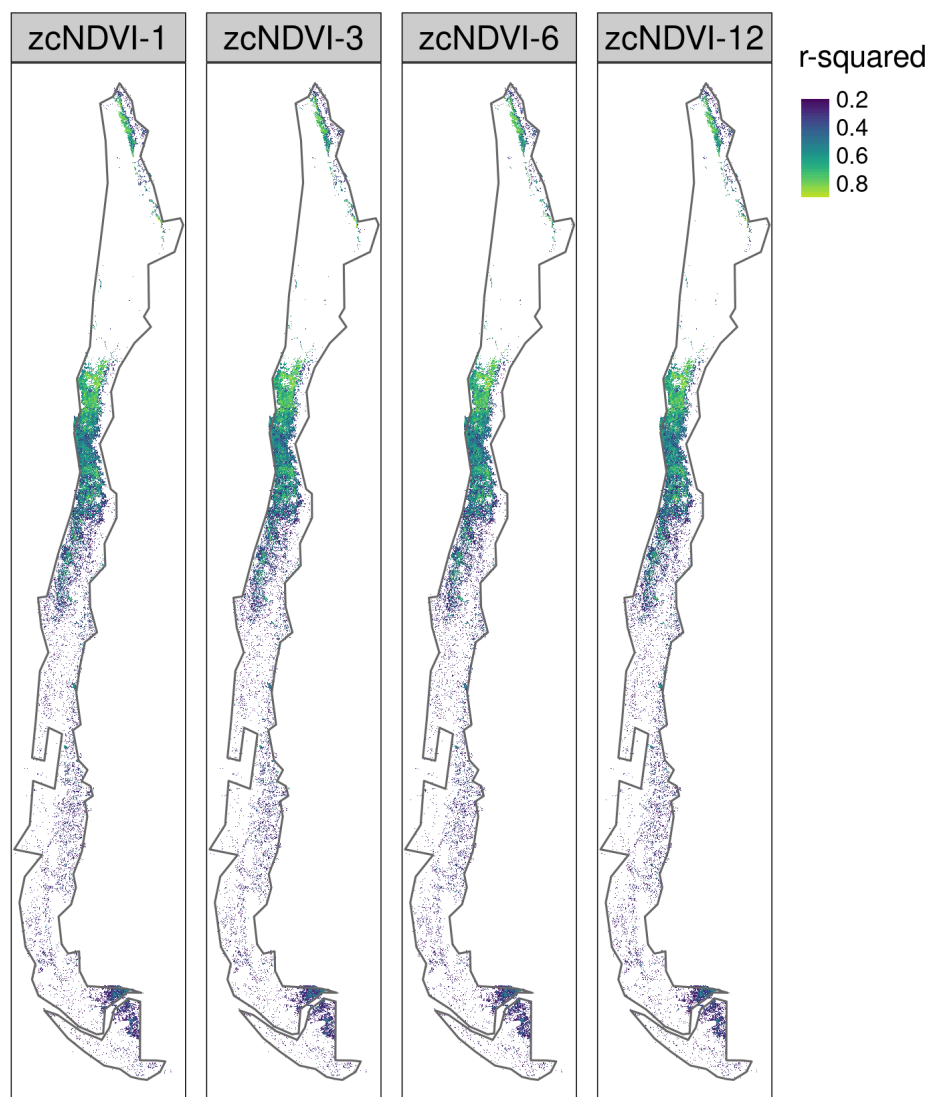Figure S2: Heatmap of trends in zcNDVI for 2000 to 2023 per macrozone and landcover macroclass.

Figure S3: Spatial variation of the r-squared values obtained from the yearly correlation of zcNDVI of 1, 3, 6, and 12 months with the net primary productivity (NPP) for continental Chile.
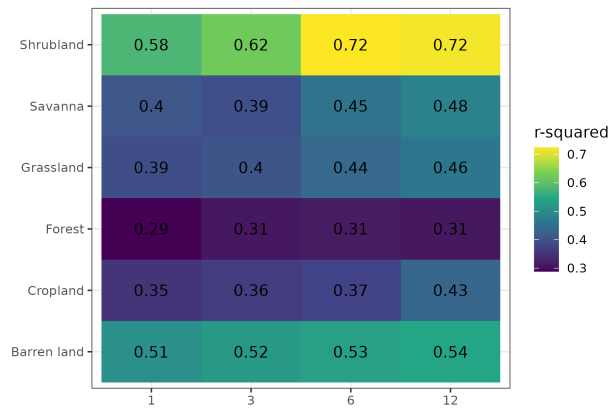
Figure S4: A heatmap showing the r-squared values obtained from the yearly correlation of zcNDVI of 1, 3, 6, and 12 months with the net primary productivity (NPP) for continental Chile.